

# Dye removal by polymer derived ceramic nanobeads

Oyku Icin, Cekdar Vakifahmetoglu\*

İzmir Institute of Technology, Department of Materials Science and Engineering, İzmir, Turkey

## ARTICLE INFO

### Keywords:

Silicon oxycarbide  
Titanium dioxide  
Coating  
Methylene blue  
Photocatalysis

## ABSTRACT

Emulsion processed polymer derived ceramic (PDC) nanobeads are used for Methylene Blue dye removal from aqueous solutions. The PDC nanobeads, produced at 600 °C and 1200 °C pyrolysis, are subsequently coated with titania (anatase). Titania-coated nanobeads show less than 35%, i.e., limited dye adsorption capability in dark. Instead, enhanced total removal efficiency (~97%) is obtained when the initial adsorption is succeeded by photodegradation under UV. Direct reusability tests show that even after the third cycle, very high regeneration efficiencies being above 92% are observed for titania-coated nanobeads.

## 1. Introduction

Widespread industrial (textile, cosmetics, pharmaceutical, food, paper, leathers, and paint industry) use of dyes causes severe pollution in the water sources resulting in a serious threat to the ecosystem [1–4]. Currently, adsorption and photocatalytic degradation are considered among the simplest, greenest, and most economical wastewater treatment approaches [3–6]. Titanium dioxide, especially the anatase polymorph, has a high potential for photocatalysts of wastewater treatment owing to decent conversion performance, hydrophilic structure, chemical and photo-stability, low toxicity, and cost [7–10].

In photocatalytic applications, titania has been employed as particulates [11], in composites [12,13], as coating [14,15], and in the porous substrates [16–19]. While it has been processed in various forms, there are some drawbacks due to separation and recycling difficulties when the fine powders were tested in photocatalytic degradation applications [20]. As a remedy, substrates were used to be coated to produce higher stability core/shell particles [20–27]. In this regard, there are only a few works that reported the formation of titania-coated polymer derived ceramics (PDCs) [13,28–30]. From those, while the authors produced titania-coated SiCN core-shell structures, no data was demonstrated regarding photocatalytic efficiency [29,30]. Instead, Awin et al. [28] studied both adsorption and photocatalytic degradation of organic dyes by using titania-coated monolithic silicon oxycarbide (SiOC) ceramics. It was postulated that the photocatalytic performance was enhanced because of mesoporous structure (higher adsorption capacity), reduction in bandgap (due to Ti–O–C/TiC) and/or the heterojunction between crystalline TiO<sub>2</sub> and the amorphous SiOC phase. In another work [13],

titania was directly incorporated in the polymer precursor to obtain SiOC/TiO<sub>2</sub> ceramic composites, while only limited removal efficiency was documented.

Different forms of SiOC ceramics (foams, membranes, aerogels, beads, etc.) have already been manufactured because of their high potential as high-temperature catalysts and filtration [31–36]. Porous SiOCs have also been used as a substrate for photocatalysis applications owing to strong chemical stability and oxidation resistance [13,28,37]. Although the formation of spherical SiOC particles has been proposed by following sol-gel [38,39], nano-precipitation [40], and emulsion [41,42], there are very limited publications [39,43–45] in which submicron PDC particles were able to be formed and tested for applications. As far as the authors are aware, titania-coated PDC nanobeads have never been utilized for dye removal from aqueous solutions. Accordingly, in this work, the aim was directed to demonstrate a facile synthesis route to obtain ceramer (CERAmic + polyMER [46,47]) and SiOC nanobeads (NBs), together with the adsorption and the photocatalytic degradation efficiency of both as-is and anatase titania-coated PDC nanobeads by using a model organic dye methylene blue (MB).

## 2. Experimental procedure

### 2.1. Sample preparation

Both ceramer and SiOC NBs were produced via the oil in water (o/w) emulsion method by using commercial polymethylsilsesquioxane (PMS) preceramic polymer (MK Belsil, Wacker GmbH, Burghausen, Germany). As a water phase, 80 mL of the deionized (DI) water (Ultrapure Type-I,

\* Corresponding author.

E-mail addresses: [cekdarvakifahmetoglu@iyte.edu.tr](mailto:cekdarvakifahmetoglu@iyte.edu.tr), [cvahmetoglu@gmail.com](mailto:cvahmetoglu@gmail.com) (C. Vakifahmetoglu).

18.2 M $\Omega$  cm at 25 °C, Millipak Direct-Q® 8 UV water purification system), and 0.8 g of surfactant (Pluronic F127, Sigma, CAS:9003-11-6, USA) were mixed with at 500 rpm for 20 min. While for oil phase 5 g of PMS and 7 mL of Toluene (Merck, EMSURE grade, CAS: 108-88-3, Germany) were mixed at 500 rpm for 10 min. The oil phase was added dropwise into the water phase and stirred for 30 min, followed by a transfer into the ice bath to apply an ultrasonic probe sonication (QSonica, Q500 system Sonicator) with 50% amplitude for 5 min, 5 s on and off. With the addition of Tin catalyst while continuing to stir for an additional 3 min. After obtaining milky emulsion, the curing was conducted for 18 h at 140 °C in an atmospheric oven. Samples were then ground in the mortar, followed by the pyrolysis at 600 °C and 1200 °C in an alumina tube furnace (PROTERM PTF 16/75/450, Ankara, Turkey) under Ar flow using the heating rate of 2 °C/min, a flow rate of 200 mL/min, and 2 h dwell time.

To prepare titania-coated PDC NBs, first 0.425 mL of Titanium(IV) n-butoxide (Alfa Aesar, 99+%, CAS:5593-70-4) was slowly added into 20 mL of absolute ethanol. 0.4 g of NBs substrate was then mixed with already prepared titania precursor sol for 24 h at room temperature (RT). At the end of the mixing, samples were degassed with an ultrasonic bath for 30 min, dried at 80 °C, and heat-treated at 450 °C/air atmosphere for 4 h at the peak temperature to obtain the photocatalytically active (anatase) titanium dioxide-coated NBs. At the end of the final heat treatment procedure, an average of 0.035  $\pm$  0.007 g of weight gain was measured for PDC NBs, attributed as the mean titania coating. For comparative analysis TiO<sub>2</sub> (anatase) powder was separately synthesized using the same chemicals and procedure applied to obtain such coating for NBs.

## 2.2. Characterization

The morphological characterization of samples was performed by using a scanning electron microscope (SEM; FEI Quanta 250 FEG, Hillsboro, OR, USA) equipped with an energy dispersive X-ray spectrometer (EDX, Oxford instruments, Aztec) for chemical analysis and transmission electron microscopy (TEM, JEOL JEM-2100, Tokyo, Japan) operating at 200 kV. All samples were sputter-coated with ~10 nm layer of Au (Emitech K550X sputter coater, Quorum Technologies, UK), prior to SEM analysis. Particle size distributions were then obtained by using the ImageJ software (ImageJ 1.52a, National Institutes of Health, USA) applied on the SEM images, an average of 200 measurements were done for each sample set, and stereological equation  $D_{\text{sphere}} = D_{\text{circle}}/0.78566$  was applied to convert the data to 3D [48].

The external surface area of the samples was calculated by using  $[(A_{\text{sphere}})/(\delta_{\text{SiOC}} * V_{\text{sphere}})]$  [49] for which the average diameter of the NBs was obtained from the particle size measurements, taking the true density of SiOC as 1.17 [50] and 2.1 g/cm<sup>3</sup> [51] for samples pyrolyzed at 600 and 1200 °C, respectively.

X-ray diffraction (XRD, Philips X'Pert Pro) data were collected by using the CuK $\alpha$  radiation (between 2 $\theta$ ; 10°-90°, step counting time of 3 s and scan of 0.05°). The XRD patterns were plotted after normalization. Fourier transform infrared spectra (FTIR, Perkin Elmer Spectrum 100) were recorded in the range 450–4000 cm<sup>-1</sup> to investigate the structural features. The decomposition behavior of polymeric beads was studied by thermal gravimetric analysis (TGA, Perkin Elmer Diamond TG/DTA, USA) with a 5 °C/min heating rate in an inert atmosphere. Nitrogen (N<sub>2</sub>) gas adsorption-desorption analyses were done by Gemini V (Micromeritics, Norcross, GA, USA). The samples were degassed at 200 °C for 24 h before analysis. Specific surface area (SSA) was determined from a BET (Brunauer–Emmett–Teller) analysis.

In order to investigate the effect of pyrolysis temperature on the wetting behavior of ceramer and SiOC samples, static water contact angle measurements were carried out using the sessile-drop technique (Attension Theta Lite 101 Biolin Scientific). X-band electron paramagnetic resonance (EPR) spectroscopy measurements were done by using a benchtop spectrometer (CMS 8400, Adani) at room temperature

in quartz tubes [52].

For all MB removal experiments (adsorption and photocatalytic degradation), 15 mg sample powder was dispersed in 30 mL of the prepared 5 ppm MB aqueous solution by magnetic stirring at 500 rpm. 2 mL of the solution was taken at certain intervals (from 2 to 24 h) and (up to 6 h) for adsorption and photocatalytic degradation, respectively. Analyses were conducted by measuring (the samples were taken from the parallel beakers separately) changes at major absorbance peak (664 nm) of MB solutions via UV–Vis spectrometer (UV2550, SHIMADZU). According to Beer-Lambert law [53], the concentration and absorbance values of the solution have a linear relationship. Concentration values were calculated by converting measured absorbance values using the Beer-Lambert law. Primarily, samples were subjected to adsorption tests (in the dark) while mixing at 500 rpm for 2 h to achieve equilibrium. Following adsorption, photocatalytic degradation measurements were carried out by using a 300W UV lamp irradiation (5% UVA, 1% UVB, and 94% Vis, Osram Ultra-Vitalux) with a wavelength at 280–400 nm in a homemade UV cabin system with air cooling. The distance between the light source and beakers was set as 20 cm. The degradation efficiency of all samples was computed using  $DE: [(C_0 - C_t)/C_0] * 100$  for which  $C_0$  and  $C_t$  are the initial and concentration at a specified time, respectively. Adsorption capacity ( $q_t$ ) was calculated with  $[(C_0 - C_t) * V]/m$  for which  $V$  is the volume of the solution, and  $m$  is adsorbent weight. For each sample, three independent measurements were conducted to determine mean and standard deviation values ( $\pm$ ). The reusability experiments were performed without any further regeneration processes (heat treatment, dissolution, etc.) in three cycles, repeated under the same conditions.

## 3. Results and discussion

### 3.1. Morphological analysis

The SEM images obtained from cured and pyrolyzed samples are given in Fig. 1. As can be seen from Fig. 1(a), homogeneously distributed polymeric spheres were kept their shape after pyrolysis, see Fig. 1(b-d).

While the morphology was not much altered, calculated volumetric shrinkage increased from 15.8% to 76.3% with the increase in the pyrolysis temperature (from 600 °C to 1200 °C). The particle size distributions of both polymeric and ceramic beads are demonstrated in Fig. 2 (a). The average particle size of the cured preceramic beads was measured as 336  $\pm$  102 nm. After pyrolysis, the average size decreased first to 303  $\pm$  115 nm for NB600, and then to 204  $\pm$  70 nm for NB1200.

TGA data obtained from the polymeric NBs is given in Fig. 2(b). The largest weight loss occurred in between 600 and 800 °C because of ceramization. Polymeric beads had a weight loss of 18.7%, corresponding to a ceramic yield of 81.3% at the peak test temperature (1200 °C), similar to the calculated value of 80.2%.

The effect of the pyrolysis temperature on the wetting behavior was analyzed by measuring the contact angle (CA). CA was decreased from 114  $\pm$  40° (Fig. 3(a)) to 27  $\pm$  10° (Fig. 3(b)) when the heat treatment temperature was raised from 600 °C to 1200 °C, indicating a transformation from a hydrophobic surface to a hydrophilic one. Xu et al. [54] reported that a decrease in the contact angle at higher pyrolysis temperatures was an indication of Si–CH<sub>3</sub> disappearance. Besides, pyrolysis at above 1000 °C, surface Si–OH groups make the material more hydrophilic [55,56]. Titania-coated samples were also tested to investigate the effect of coating on wettability. The hydrophobic surface of the NB600 changed to a hydrophilic one with the contact angle 32  $\pm$  0.2° (Fig. 3(c)) following titania coating, whereas no change was seen in wettability characteristics for the NB1200Ti sample, Fig. 3(d).

### 3.2. Structural characterizations

The FTIR spectra of polymeric, pyrolyzed, and TiO<sub>2</sub>-coated ceramer and SiOC NBs are given in Fig. 4(a). In the spectra of polymeric NBs, the

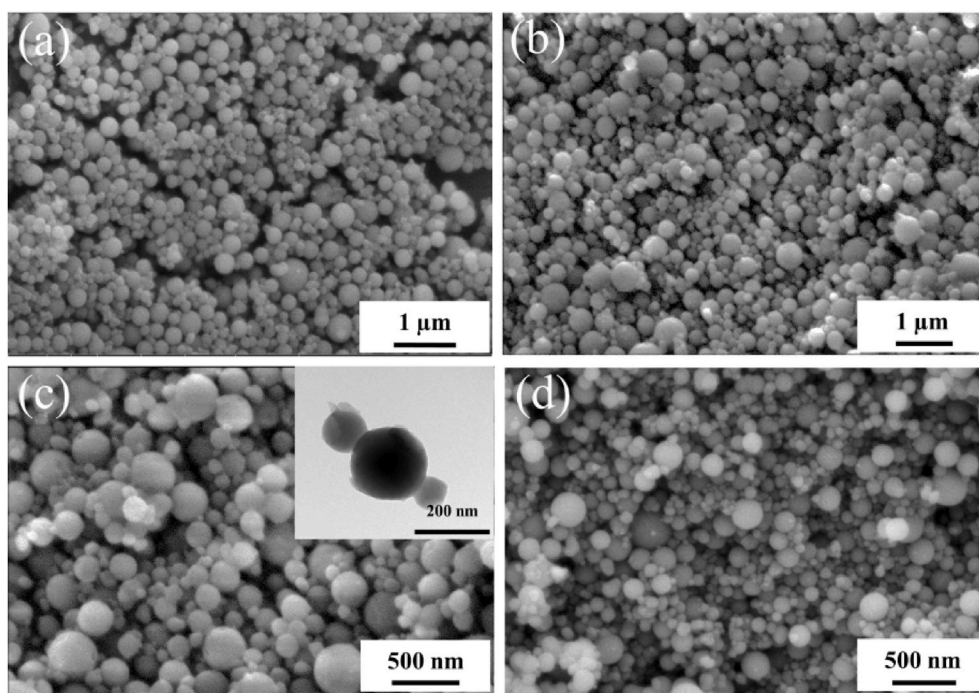


**Fig. 1.** SEM images of the formed samples; (a) polymeric NBs, (b) sample pyrolyzed at 600 °C: NB600, (c) higher magnification image of NB600 (the inset shows the TEM images of NB600), and (d) sample pyrolyzed at 1200 °C: NB1200.

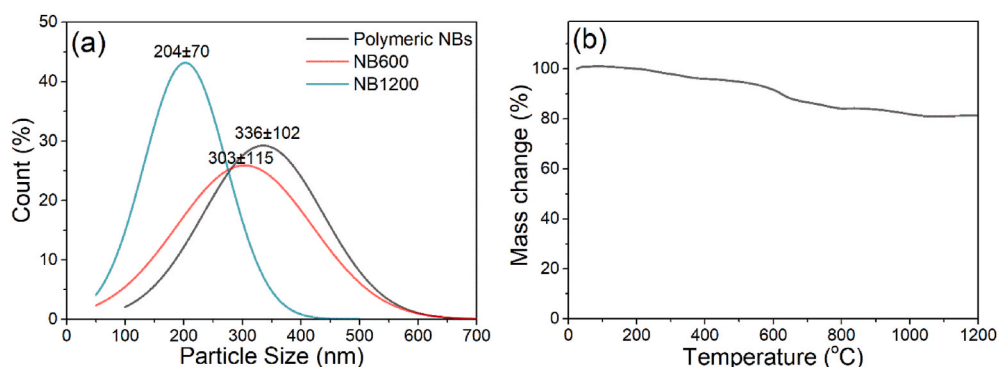


**Fig. 2.** (a) Particle size (diameter) distributions of polymeric NBs, and samples obtained by the pyrolysis at 600 and 1200 °C for 2 h at peak temperature, (b) TGA analysis of the polymeric NBs taken with 5 °C/min; N<sub>2</sub> flow 0.05 L/min.

peaks assigned to the Si–CH<sub>3</sub> bond vibration located around 774 cm<sup>-1</sup> and 1274 cm<sup>-1</sup> can be seen. After pyrolysis, the intensity of these peaks reduced, and with the increase in the heat treatment temperature, they disappear. The sample obtained by 1200 °C pyrolysis (NB1200) had a spectrum with Si–C and Si–O stretching vibration centering around 805 cm<sup>-1</sup> [48] and also broad peak ~1050 cm<sup>-1</sup>, corresponding to Si–O stretching in Si–O–Si/Si–O–C [41]. In addition, the broadband around 3500 cm<sup>-1</sup> is referred to as O–H stretching [57]. The spectra of TiO<sub>2</sub>-coated ceramer and SiOC NBs were similar to those of the uncoated ones with no observable signs for Ti-related bonds due to the overlapping [16, 28].

The XRD patterns for bare NBs and TiO<sub>2</sub>-coated NBs are shown in Fig. 4(b). XRD analyses show no crystalline phases for any SiOC-NB substrates, only a broad Bragg reflection from ~10° and 30° (2θ), associated with amorphous silicates [58]. When the TiO<sub>2</sub>-coated samples are examined, the existence of anatase titanium dioxide can be supported by the new peaks evolved around at 2θ of 25°, 37°, 48°, 54°, 55°, and 63°.

The N<sub>2</sub> sorption isotherms recorded on the bare and titania-coated samples are reported in Fig. 5(a). The isotherm for the 600 °C

pyrolyzed sample resembles Type IV based on IUPAC classification, instead, the sample obtained from the 1200 °C treatment shows Type II. The sample coded as NB600 showed the highest yield and specific surface area (SSA), being 87.5% and 370.9 m<sup>2</sup>/g, respectively. The latter was mostly due to transient intraparticular nanoscale porosity formed from the release of gaseous byproducts during ceramization at 600 °C heat treatment [59]. When the pyrolysis temperature was increased, i.e., upon the completion of the polymer-ceramic transition, such nanoscale pores shrunk and SSA decreased to 23.5 m<sup>2</sup>/g with 80.2% ceramic yield at 1200 °C (NB1200) (see later TGA info as well). The external surface area of NB600 and NB1200 samples were calculated as 9.5 and 13.9 m<sup>2</sup>/g, respectively. Although the value is around the one obtained from the BET for the NB1200, it is clearly different for the NB600 corroborating the intraparticular porosity observed for the sample. While titania coating caused a probable partial micropore closure (see later for N<sub>2</sub> sorption isotherms), resulting in a slight surface area decrease for NB600 (296 m<sup>2</sup>/g), the NB1200Ti sample (35.9 m<sup>2</sup>/g) demonstrated to have a higher surface area, like previous observations [22,60].

EPR analysis was performed to visualize the presence of the free carbon phase in the formed PDC structures. In Fig. 5(b), EPR spectra of

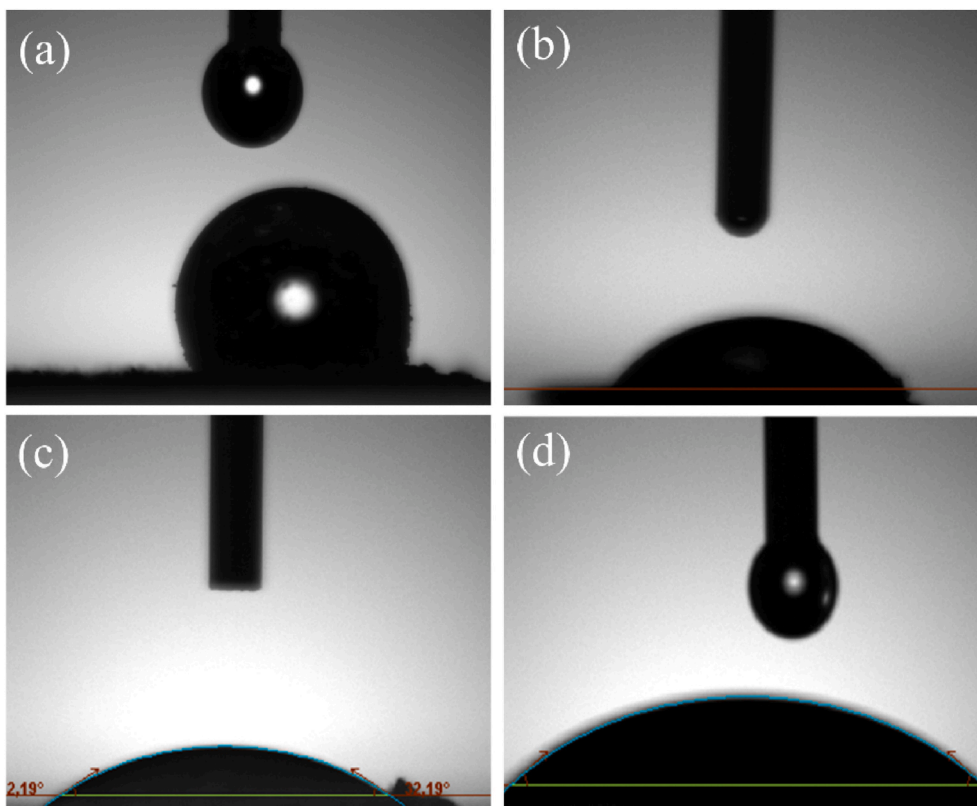


Fig. 3. Wetting angle test results; (a) NB600 CA [°]:  $114 \pm 40$ , (b) NB1200 CA [°]:  $27 \pm 10$ , (c) NB600Ti CA [°]:  $32 \pm 0.2$ , and (d) NB1200Ti CA [°]:  $38 \pm 0.2$ .

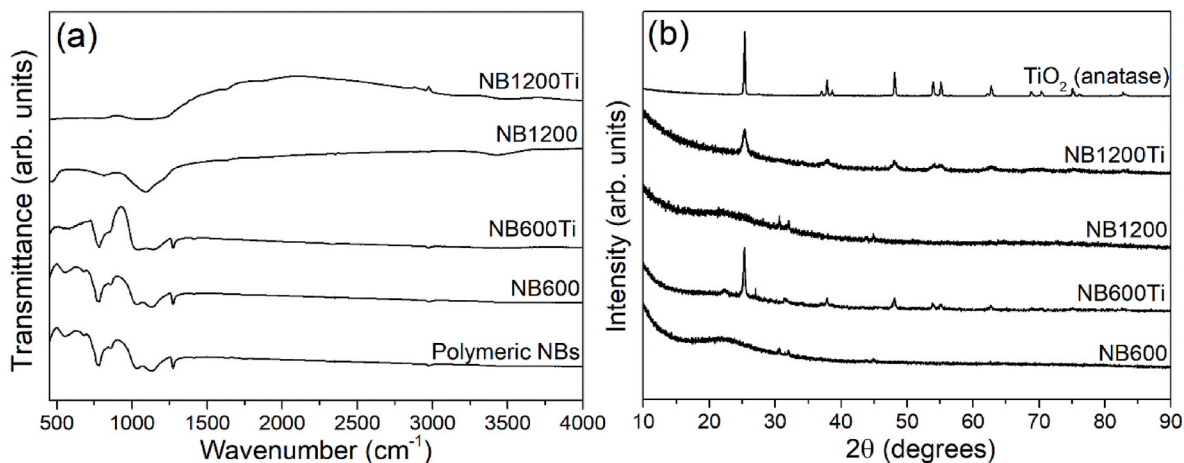


Fig. 4. Normalized; (a) FTIR spectra of polymeric, pyrolyzed and  $\text{TiO}_2$ -coated NBs, and (b) XRD patterns of bare and  $\text{TiO}_2$ -coated ceramer and SiOC NBs produced by  $600^\circ\text{C}$ , and  $1200^\circ\text{C}$  pyrolysis. At the top of the experimental data, reference reflection marks for pure anatase  $\text{TiO}_2$  (ICDD PDF #00-021-1272) are given.

uncoated and  $\text{TiO}_2$ -coated samples are given after normalization with the amount of the samples. The sharp signals with a g-factor of 2.00025 were obtained. The signal intensity of NB1200 (representing the number of spins) is clearly higher than that of the NB600, similarly observed for titania-coated ones. In the previous study [61] about carbon distribution in SiOC glasses, the majority of the paramagnetic centers were attributed to carbon g-factor due to carbon related dangling bonds. While EPR spectroscopy demonstrated different signals, intensities related to the dangling bonds in the obtained PDCs, further research is needed to provide their exact influence on the total MB removal efficiency (see later).

### 3.3. MB removal tests

Fig. 6(a) shows the MB adsorption efficiency (in dark) of the samples as a function of pyrolysis temperature and time. While the sample NB600 had the highest SSA ( $370.9\text{ m}^2/\text{g}$ ), it adsorbed only  $5.1 \pm 1.6\%$  of the dye which did not much alter with prolonged testing time. When the pyrolysis temperature was increased to  $1200^\circ\text{C}$ , the surface area decreased more than tenfold but adsorption efficiency increased. At the end of the 24 h period, NB1200 showed the highest adsorption capability being around 82%. This indicated that the lower adsorption efficacy of the  $600^\circ\text{C}$  treated samples was probably due to the combination of factors including hydrophobic behavior, lack of free carbon precipitation, and surface silanol groups as similarly seen in other low

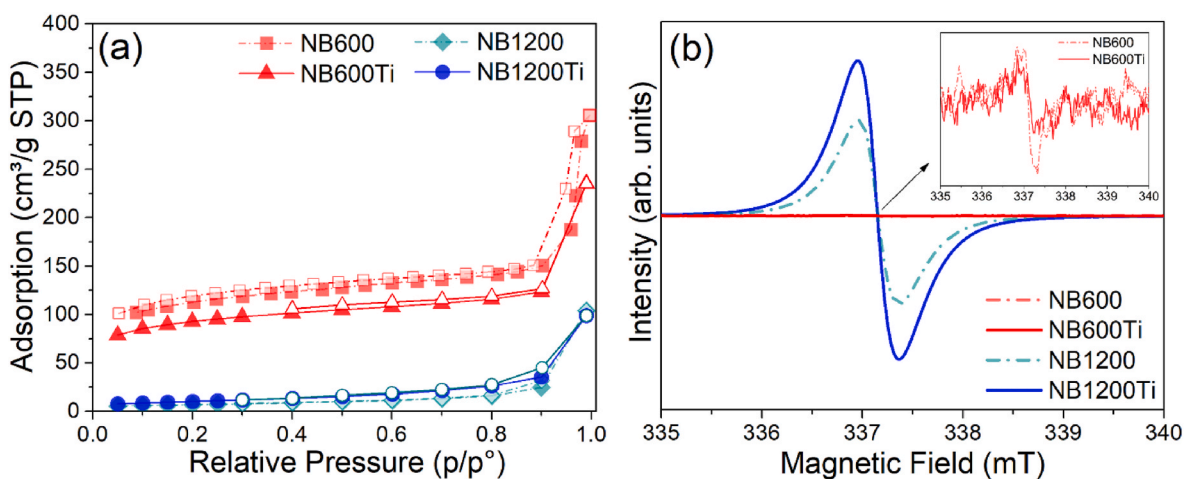


Fig. 5. (a) N<sub>2</sub> sorption isotherms, and (b) X-band EPR spectra of the bare and TiO<sub>2</sub>-coated NBs.

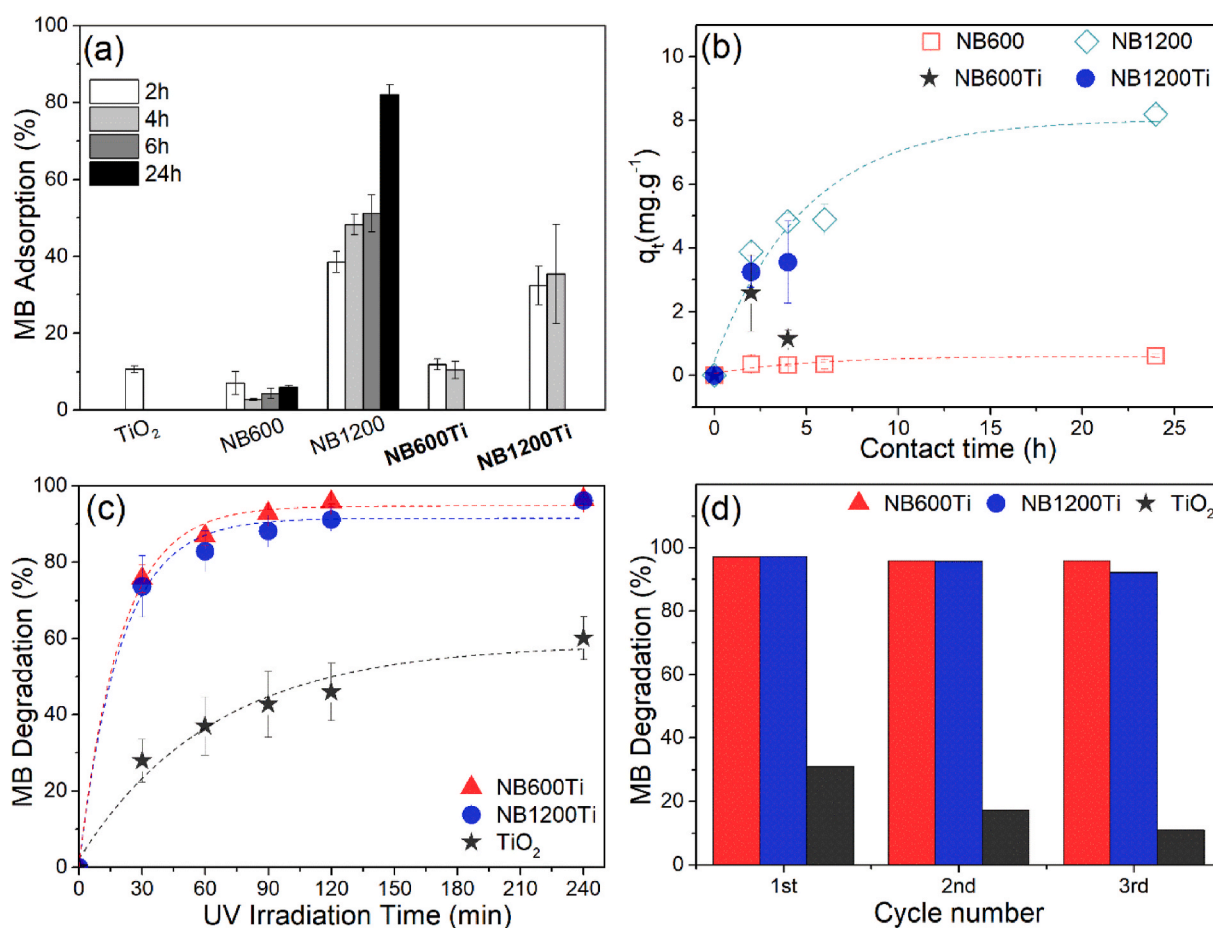


Fig. 6. (a) MB adsorption efficiency in the dark with different contact times for NB600, NB1200, NB600Ti, NB1200Ti, and TiO<sub>2</sub> powder, (b) effect of contact time on MB adsorption capacity for uncoated and TiO<sub>2</sub>-coated NBs, (c) MB degradation efficiency under UV light irradiation for NB600Ti, NB1200Ti, and TiO<sub>2</sub> powder (the dashed lines represent the exponential non-linear fitting resulting with R<sup>2</sup> > 0.7370), and (d) reusability of the photocatalyst.

temperature pyrolyzed samples [62]. Titania-coated samples demonstrated similar behavior, i.e., with the increase in pyrolysis temperature, adsorption efficiency increased, see Fig. 6(a).

The effect of contact time on MB adsorption capacity is depicted in Fig. 6(b). Adsorption equilibrium was achieved after 2 h for NB600 with 0.6 mg g<sup>-1</sup>, while the capacity of NB1200 showed a gradual rise as the contact time was increased, reaching 8.2 mg g<sup>-1</sup> at the end of 24 h. Fig. 6

(c) demonstrates the total MB removal efficiency of unsupported anatase titania powder and titania-coated samples subjected to adsorption in dark for 2 h, followed by UV irradiation for 4 h. It is important to note that when no sample was added into the aqueous solution, the (self-)degradation of MB dye under UV irradiation of 4 h was found to be around 12%.

EDX analysis (data not shown for brevity) indicated that TiO<sub>2</sub>-coated

samples contain only Si, O, C, and Ti elements. The latter was detected approximately 4.14 wt% for NB600Ti and 6.02 wt% for NB1200Ti. This makes around 1.04–1.51 mg of titania, close to the calculated values after the coating and heat treatment (1.46 and 0.98 mg). In photocatalytic experiments, even when a higher amount of synthesized titania powder (3 mg) was tested, total MB removal efficiency (adsorption, followed by photodegradation under UV) of the unsupported as-is titania powder reached only around 60% (see Fig. 6(c)). Although NB600Ti and NB1200Ti exhibited limited adsorption capability being <35% in the dark, total removal efficiencies were quite high (~97%) under identical test conditions. This implies that the degradation capability of the titania-coated samples, regardless of the NB core type and their SSA, was majorly affected by the amount of the applied titania coating [63,64]. Besides, the utilization of PDC NBs as a substrate for TiO<sub>2</sub> coating was clearly effective in getting higher total removal efficiencies under UV irradiation compared to un-supported as-is titania [65]. Further studies are certainly needed to elucidate the exact mechanism causing such a result which could be related to the formation of Ti–O–C/TiC bonds i.e., reduction in the bandgap and/or the heterojunction between crystalline TiO<sub>2</sub> and the amorphous SiOC phase (reduced recombination rate of the electron-hole pair) as in the case for previous work [28].

The re-usability is important for photocatalysis to minimize process cost, time, and additional waste generation. Here the samples were tested without any further regeneration process such as thermal or acid/base treatment, in three cycles under identical test conditions to assess their reusability. After the completion of each cycle, powders were simply washed and dried at 90 °C in the atmospheric oven. The degradation efficiency of unsupported as-is TiO<sub>2</sub> powder produced in the same way, decreased to 11% after the third cycle, due probably to the catalyst poisoning, i.e., reduction of active sites [66]. Instead, the photocatalytic efficiency of NB600Ti and NB1200Ti did not show any noticeable loss, as given in Fig. 6(d), the performances of titania-coated ceramer/SiOC samples were always above 92% even after the third cycle.

#### 4. Conclusions

Both ceramer (NB600) and SiOC (NB1200) nanobeads were produced via simple oil in water emulsion processing, followed by curing and pyrolysis (600 and 1200 °C). Not only the reduction in the specific surface area but also hydrophobic to the hydrophilic transformation of the bead surfaces were observed with the increase in pyrolysis temperature. The formed NBs were then coated with a titanium precursor, heat-treated to obtain the anatase titania coat layer, i.e., formation of ceramer/SiOC core, titania shell NBs. Methylene blue (MB) removal tests indicated limited adsorption capability being around 10% and 35% for titania-coated ceramer (NB600Ti) and SiOC (NB1200Ti), respectively. The total removal efficiency (adsorption in dark for 2 h, followed by photodegradation under UV for 4 h) reached around 97% irrespective of the tested titania-coated NB type. This was below 60% for as-is anatase TiO<sub>2</sub> powder, prepared and tested under identical conditions, revealing the positive effect of the core/shell approach. Direct reusability studies (without any regeneration processes) for core/shell NBs demonstrated that the efficiency decreased only slightly from 97% to 95% for NB600Ti and to 92% for NB1200Ti after the third cycle, displaying decent direct reusability toward dye removal.

#### Declaration of competing interest

The authors declare that they have no known competing financial interests or personal relationships that could have appeared to influence the work reported in this paper.

#### Acknowledgments

The author wishes to express sincere appreciation to Dr. Yasar

Akdogan, Dr. Umit Hakan Yildiz, and Soner Karabacak from Izmir Institute of Technology. Cekdar Vakif Ahmetoglu acknowledges the support of the Alexander von Humboldt (AvH) Foundation.

#### References

- [1] Z. Wu, W. Huang, X. Shan, Z. Li, Preparation of a porous graphene oxide/alkali lignin aerogel composite and its adsorption properties for methylene blue, *Int. J. Biol. Macromol.* 143 (2020) 325–333, <https://doi.org/10.1016/j.ijbiomac.2019.12.017>.
- [2] J. Li, L. Zheng, H. Liu, A novel carbon aerogel prepared for adsorption of copper (II) ion in water, *J. Porous Mater.* 24 (2017) 1575–1580, <https://doi.org/10.1007/s10934-017-0397-y>.
- [3] T.-H. Liou, M.-H. Lin, Characterization of graphene oxide supported porous silica for effectively enhancing adsorption of dyes, *Separ. Sci. Technol.* 55 (2020) 431–443, <https://doi.org/10.1080/01496395.2019.1577274>.
- [4] J. Pan, J. Ren, Y. Xie, X. Wei, Y. Guan, X. Yan, H. Tang, X. Cheng, Porous SiOC composites fabricated from preceramic polymers and wood powders for efficient dye adsorption and removal, *Res. Chem. Intermed.* 43 (2017) 3813–3832, <https://doi.org/10.1007/s11164-016-2850-y>.
- [5] A. Charanpahari, N. Gupta, V. Devthade, S. Ghugal, J. Bhatt, Ecofriendly nanomaterials for sustainable photocatalytic decontamination of organics and bacteria, in: L. Martínez, O. Kharissova, B. Kharisov (Eds.), *Handbook of Ecomaterials*, Springer, Cham, 2018, pp. 1–29, [https://doi.org/10.1007/978-3-319-48281-1\\_179-1](https://doi.org/10.1007/978-3-319-48281-1_179-1).
- [6] T. Fazal, A. Razaq, F. Javed, A. Hafeez, N. Rashid, U.S. Amjad, M.S.U. Rehman, A. Faisal, F. Rehman, Integrating adsorption and photocatalysis: a cost effective strategy for textile wastewater treatment using hybrid biochar-TiO<sub>2</sub> composite, *J. Hazard Mater.* 390 (2020) 121623, <https://doi.org/10.1016/j.jhazmat.2019.12.1623>.
- [7] D.S. Bhatkhande, V.G. Pangarkar, A.A.C.M. Beenackers, Photocatalytic degradation for environmental applications—a review, *J. Chem. Technol. Biotechnol.: Int. Res. Process. Environ. Clean Technol.* 77 (2002) 102–116, <https://doi.org/10.1002/jctb.532>.
- [8] M. Umar, H.A. Aziz, Photocatalytic degradation of organic pollutants in water, in: M.N. Rashed (Ed.), *Organic Pollutants—Monitoring, Risk and Treatment*, IntechOpen, vol. 8, 2013, pp. 196–197, <https://doi.org/10.5772/53699>.
- [9] R. Wang, K. Shi, D. Huang, J. Zhang, S. An, Synthesis and degradation kinetics of TiO<sub>2</sub>/GO composites with highly efficient activity for adsorption and photocatalytic degradation of MB, *Sci. Rep.* 9 (2019) 1–9, <https://doi.org/10.1038/s41598-019-54320-w>.
- [10] S. Sakthivel, B. Neppolian, M. Shankar, B. Arabindoo, M. Palanichamy, V. Murugesan, Solar photocatalytic degradation of azo dye: comparison of photocatalytic efficiency of ZnO and TiO<sub>2</sub>, *Sol. Energy Mater. Sol. Cells* 77 (2003) 65–82, [https://doi.org/10.1016/S0927-0248\(02\)00255-6](https://doi.org/10.1016/S0927-0248(02)00255-6).
- [11] X. Cui, J. Wang, X. Zhang, Q. Wang, M. Song, J. Chai, Preparation of nano-TiO<sub>2</sub> by a surfactant-free microemulsion–hydrothermal method and its photocatalytic activity, *Langmuir* 35 (2019) 9255–9263, <https://doi.org/10.1021/acs.langmuir.9b01392>.
- [12] H. Zhang, X. Lv, Y. Li, Y. Wang, J. Li, P25-Graphene composite as a high performance photocatalyst, *ACS Nano* 4 (2010) 380–386, <https://doi.org/10.1021/nn901221k>.
- [13] M. Hojamberdiev, R.M. Prasad, K. Morita, Y. Zhu, M.A. Schiavon, A. Gurlo, R. Riedel, Template-free synthesis of polymer-derived mesoporous SiOC/TiO<sub>2</sub> and SiOC/N-doped TiO<sub>2</sub> ceramic composites for application in the removal of organic dyes from contaminated water, *Appl. Catal. B Environ.* 115 (2012) 303–313, <https://doi.org/10.1016/j.apcatb.2011.12.036>.
- [14] Y. Li, X. Li, J. Li, J. Yin, Photocatalytic degradation of methyl orange by TiO<sub>2</sub>-coated activated carbon and kinetic study, *Water Res.* 40 (2006) 1119–1126, <https://doi.org/10.1016/j.watres.2005.12.042>.
- [15] F.B. Löffler, F.J. Altermann, E.C. Bucharsky, K.G. Schell, M.L. Vera, H. Traid, A. Dwojak, M.I. Litter, Morphological characterization and photocatalytic efficiency measurements of pure silica transparent open-cell sponges coated with TiO<sub>2</sub>, *Int. J. Appl. Ceram. Technol.* 17 (2020) 1930–1939, <https://doi.org/10.1111/ijac.13504>.
- [16] E.B. Ertus, C. Vakifahmetoglu, A. Ozturk, Enhanced methylene blue removal efficiency of TiO<sub>2</sub> embedded porous glass, *J. Eur. Ceram. Soc.* 41 (2020) 1530–1536, <https://doi.org/10.1016/j.jeurceramsoc.2020.09.047>.
- [17] C. Jiang, K.Y. Lee, C.M.A. Parlett, M.K. Bayazit, C.C. Lau, Q. Ruan, S.J.A. Moniz, A. F. Lee, J. Tang, Size-controlled TiO<sub>2</sub> nanoparticles on porous hosts for enhanced photocatalytic hydrogen production, *Appl. Catal. Gen.* 521 (2016) 133–139, <https://doi.org/10.1016/j.apcata.2015.12.004>.
- [18] T. Yildiz, H.C. Yatmaz, K. Ozturk, Anatase TiO<sub>2</sub> powder immobilized on reticulated Al<sub>2</sub>O<sub>3</sub> ceramics as a photocatalyst for degradation of RO16 azo dye, *Ceram. Int.* 46 (2020) 8651–8657, <https://doi.org/10.1016/j.ceramint.2019.12.098>.
- [19] X. Wang, Y. Liu, Z. Hu, Y. Chen, W. Liu, G. Zhao, Degradation of methyl orange by composite photocatalysts nano-TiO<sub>2</sub> immobilized on activated carbons of different porosities, *J. Hazard Mater.* 169 (2009) 1061–1067, <https://doi.org/10.1016/j.jhazmat.2009.04.058>.
- [20] J. Zheng, Y. Wu, Q. Zhang, Y. Li, C. Wang, Y. Zhou, Direct liquid phase deposition fabrication of waxberry-like magnetic Fe<sub>3</sub>O<sub>4</sub>@TiO<sub>2</sub> core-shell microspheres, *Mater. Chem. Phys.* 181 (2016) 391–396, <https://doi.org/10.1016/j.matchemphys.2016.06.074>.

- [21] J. Lee, M. Othman, Y. Eom, T. Lee, W. Kim, J. Kim, The effects of sonification and TiO<sub>2</sub> deposition on the micro-characteristics of the thermally treated SiO<sub>2</sub>/TiO<sub>2</sub> spherical core-shell particles for photo-catalysis of methyl orange, *Microporous Mesoporous Mater.* 116 (2008) 561–568, <https://doi.org/10.1016/j.micromeso.2008.05.017>.
- [22] E.P. Ferreira-Neto, S. Ullah, M.B. Simoes, A.P. Perissinotto, F.S. de Vicente, P.-L. M. Noeske, S.J. Ribeiro, U.P. Rodrigues-Filho, Solvent-controlled deposition of titania on silica spheres for the preparation of SiO<sub>2</sub>@TiO<sub>2</sub> core@shell nanoparticles with enhanced photocatalytic activity, *Colloid. Surface. Physicochem. Eng. Aspect.* 570 (2019) 293–305, <https://doi.org/10.1016/j.colsurfa.2019.03.036>.
- [23] A. Li, Y. Jin, D. Muggli, D.T. Pierce, H. Aranwala, G.K. Marasinghe, T. Knutson, G. Brockman, J.X. Zhao, Nanoscale effects of silica particle supports on the formation and properties of TiO<sub>2</sub> nanocatalysts, *Nanoscale* 5 (2013) 5854–5862, <https://doi.org/10.1039/C3NR01287E>.
- [24] D. Beydoun, R. Amal, G.K.-C. Low, S. McEvoy, Novel photocatalyst: titania-coated magnetite. Activity and photodissolution, *J. Phys. Chem. B* 104 (2000) 4387–4396, <https://doi.org/10.1021/jp992088c>.
- [25] K. Cendrowski, X. Chen, B. Zielinska, R. Kalenczuk, M. Rummeli, B. Buchner, R. Klingeler, E. Borowiak-Palen, Synthesis, characterization, and photocatalytic properties of core/shell mesoporous silica nanospheres supporting nanocrystalline titania, *J. Nanoparticle Res.* 13 (2011) 5899–5908, <https://doi.org/10.1007/s11051-011-0307-1>.
- [26] I. Kitsou, P. Panagopoulos, T. Maggos, M. Arkas, A. Tsetsekou, Development of SiO<sub>2</sub>@TiO<sub>2</sub> core-shell nanospheres for catalytic applications, *Appl. Surf. Sci.* 441 (2018) 223–231, <https://doi.org/10.1016/j.apsusc.2018.02.008>.
- [27] P. Rajeswari, S. Ram, D. Pradhan, Core-shell synergy and Eu<sup>3+</sup> doping in boosting charge transfer in Eu<sup>3+</sup> doped TiO<sub>2</sub>-carbon core-shell nanohybrids: sustainable synthesis and visible light-driven photocatalysis, *Appl. Surf. Sci.* 492 (2019) 473–486, <https://doi.org/10.1016/j.apsusc.2019.06.169>.
- [28] E. Wasan Awini, A. Lale, K.C.N.H. Kumar, U. Bilge Demirci, S. Bernard, R. Kumar, Novel precursor-derived meso-/macroporous TiO<sub>2</sub>/SiOC nanocomposites with highly stable anatase nanophase providing visible light photocatalytic activity and superior adsorption of organic dyes, *Materials* 11 (2018) 362, <https://doi.org/10.3390/ma11030362>.
- [29] H. Liu, H. Zhang, J. Li, W. Kang, P. Chu, A novel SiCN@TiO<sub>2</sub> core-shell ceramic microspheres derived from a polymeric precursor, *Ceram. Int.* 42 (2016) 7135–7140, <https://doi.org/10.1016/j.ceramint.2016.01.102>.
- [30] H. Liu, N. Wei, J. Li, H. Zhang, P. Chu, Synthesis of SiCN@TiO<sub>2</sub> core-shell ceramic microspheres via PDCs method, *Solid State Sci.* 76 (2018) 15–19, <https://doi.org/10.1016/j.solidstatesciences.2017.11.012>.
- [31] M.C. Bruzzoniti, M. Appendini, L. Rivoira, B. Onida, M. Del Bubba, P. Jana, G. D. Soraru, Polymer-derived ceramic aerogels as sorbent materials for the removal of organic dyes from aqueous solutions, *J. Am. Ceram. Soc.* 101 (2018) 821–830, <https://doi.org/10.1111/jace.15241>.
- [32] D. Zeydanli, S. Akman, C. Vakifahmetoglu, Polymer-derived ceramic adsorbent for pollutant removal from water, *J. Am. Ceram. Soc.* 101 (2018) 2258–2265, <https://doi.org/10.1111/jace.15423>.
- [33] J. Pan, W. Shen, Y. Zhao, H. Sun, T. Guo, Y. Cheng, N. Zhao, H. Tang, X. Yan, Difunctional hierarchical porous SiOC composites from silicone resin and rice husk for efficient adsorption and as a catalyst support, *Colloid. Surface. Physicochem. Eng. Aspect.* 584 (2020) 124041, <https://doi.org/10.1016/j.colsurfa.2019.124041>.
- [34] H. Zhang, C.L. Fidelis, A.L.T. Serva, M. Wilhelm, K. Rezwani, Water-based freeze casting: adjusting hydrophobic polymethylsiloxane for obtaining hierarchically ordered porous SiOC, *J. Am. Ceram. Soc.* 100 (2017) 1907–1918, <https://doi.org/10.1111/jace.14782>.
- [35] Z. Zhang, Y. Bao, X. Sun, K. Chen, M. Zhou, L. He, Q. Huang, Z. Huang, Z. Chai, Y. Song, Mesoporous polymer-derived ceramic membranes for water purification via a self-sacrificed template, *ACS Omega* 5 (2020) 11100–11105, <https://doi.org/10.1021/acsomega.0c01021>.
- [36] B.-B. Dong, F.-H. Wang, M.-Y. Yang, J.-L. Yu, L.-Y. Hao, X. Xu, G. Wang, S. Agathopoulos, Polymer-derived porous SiOC ceramic membranes for efficient oil-water separation and membrane distillation, *J. Membr. Sci.* 579 (2019) 111–119, <https://doi.org/10.1016/j.memsci.2019.02.066>.
- [37] M. Hojamberdiev, R.M. Prasad, K. Morita, M.A. Schiavon, R. Riedel, Polymer-derived mesoporous SiOC/ZnO nanocomposite for the purification of water contaminated with organic dyes, *Microporous Mesoporous Mater.* 151 (2012) 330–338, <https://doi.org/10.1016/j.micromeso.2011.10.015>.
- [38] M. Weinberger, J. Munding, M. Linden, M. Wohlfahrt-Mehrens, Template-derived submicrometric carbon spheres for lithium-sulfur and sodium-ion battery electrodes, *Energy Technol.* 6 (2018) 1797–1804, <https://doi.org/10.1002/ente.201700932>.
- [39] Z. Sang, D. Su, J. Wang, Y. Liu, H. Ji, Bi-continuous nanoporous carbon sphere derived from SiOC as high-performance anodes for PIBs, *Chem. Eng. J.* 381 (2020) 122677, <https://doi.org/10.1016/j.cej.2019.122677>.
- [40] Y. Chen, S. Li, Y. Luo, C. Xu, Fabrication of polycarbosilane and silicon oxycarbide microspheres with hierarchical morphology, *Solid State Sci.* 13 (2011) 1664–1667, <https://doi.org/10.1016/j.solidstatesciences.2011.06.009>.
- [41] C. Vakifahmetoglu, M. Balliana, P. Colombo, Ceramic foams and micro-beads from emulsions of a preceramic polymer, *J. Eur. Ceram. Soc.* 31 (2011) 1481–1490, <https://doi.org/10.1016/j.jeurceramsoc.2011.02.012>.
- [42] B. Dong, Y. Han, T. Wang, Z. Lei, Y. Chen, F. Wang, H. Abadikhah, S.A. Khan, L. Hao, X. Xu, R. Cao, L. Yin, S. Agathopoulos, Hard SiOC microbeads as a high-performance Lithiumion battery anode, *ACS Appl. Energy Mater.* 3 (2020) 10183–10191, <https://doi.org/10.1021/acsaem.0c01910>.
- [43] H. Shi, A. Yuan, J. Xu, Tailored synthesis of monodispersed nano/submicron porous silicon oxycarbide (SiOC) spheres with improved Li-storage performance as an anode material for Li-ion batteries, *J. Power Sources* 364 (2017) 288–298, <https://doi.org/10.1016/j.jpowsour.2017.08.051>.
- [44] V. Bakumov, M. Schwarz, E. Kroke, Emulsion processing and size control of polymer-derived spherical Si/C/O ceramic particles, *Soft Mater.* 4 (2007) 287–299, <https://doi.org/10.1080/15394450701310251>.
- [45] S. Dire, V. Tagliazucca, L. Salvadori, G.D. Soraru, Preparation of dense and porous silicon oxycarbide submicrometer-sized spheres using a modified stober process, *J. Am. Ceram. Soc.* 94 (2011) 3819–3824, <https://doi.org/10.1111/j.1551-2916.2011.04732.x>.
- [46] M. Wilhelm, C. Soltmann, D. Koch, G. Grathwohl, Ceramers—functional materials for adsorption techniques, *J. Eur. Ceram. Soc.* 25 (2005) 271–276, <https://doi.org/10.1016/j.jeurceramsoc.2004.08.008>.
- [47] C. Vakifahmetoglu, T. Semerci, A. Gurlo, G.D. Soraru, Polymer derived ceramic aerogels, *Curr. Opin. Solid State Mater. Sci.* 25 (2021) 100936, <https://doi.org/10.1016/j.cossms.2021.100936>.
- [48] T. Semerci, M.D. de Mello Innocentini, G.A. Marsola, P.R.O. Lasso, G.D. Soraru, C. Vakifahmetoglu, Hot air permeable preceramic polymer derived reticulated ceramic foams, *ACS Appl. Polym. Mater.* 2 (2020) 4118–4126, <https://doi.org/10.1021/acspap.0c00734>.
- [49] Y. Ghasemi, M. Emborg, A. Cwirzen, Estimation of specific surface area of particles based on size distribution curve, *Mag. Concr. Res.* 70 (2018) 533–540, <https://doi.org/10.1680/jmacr.17.00045>.
- [50] Z. Li, Z. Chen, J. Liu, Y. Fu, C. Liu, P. Wang, M. Jiang, C. Lao, Additive manufacturing of lightweight and high-strength polymer-derived SiOC ceramics, *Virtual Phys. Prototyp.* 15 (2020) 163–177, <https://doi.org/10.1080/17452759.2019.1710919>.
- [51] A. Guo, M. Rosso, M. Modesti, E. Maire, J. Adrien, P. Colombo, Characterization of porosity, structure, and mechanical properties of electrosput SiOC fiber mats, *J. Mater. Sci.* 50 (2015) 4221–4231, <https://doi.org/10.1007/s10853-015-8973-5>.
- [52] Y. Goksel, Y. Akdogan, Increasing spontaneous wet adhesion of DOPA with gelatin characterized by EPR spectroscopy, *Mater. Chem. Phys.* 228 (2019) 124–130, <https://doi.org/10.1016/j.matchemphys.2019.02.054>.
- [53] V. Scuderi, M.A. Buccheri, G. Impellizzeri, A. Di Mauro, G. Rappazzo, K. Bergum, B.G. Svensson, V. Privitera, Photocatalytic and antibacterial properties of titanium dioxide flat film, *Mater. Sci. Semicond. Process.* 42 (2016) 32–35, <https://doi.org/10.1016/j.mssp.2015.09.005>.
- [54] Y.-D. Xu, Z.-Y. Zhu, T.-Z. Xu, H. Abadikhah, J.-W. Wang, X. Xu, S. Agathopoulos, Fabrication and characterization of robust hydrophobic lotus leaf-like surface on Si<sub>3</sub>N<sub>4</sub> porous membrane via polymer-derived SiNCO inorganic nanoparticle modification, *Ceram. Int.* 44 (2018) 16443–16449, <https://doi.org/10.1016/j.ceramint.2018.06.058>.
- [55] M. Nakamura, M. Kobayashi, N. Kuzuya, T. Komatsu, T. Mochizuka, Hydrophilic property of SiO<sub>2</sub>/TiO<sub>2</sub> double layer films, *Thin Solid Films* 502 (2006) 121–124, <https://doi.org/10.1016/j.tsf.2005.07.254>.
- [56] N. Wu, L.Y. Wan, Y. Wang, F. Ko, Conversion of hydrophilic SiOC nanofibrous membrane to robust hydrophobic materials by introducing palladium, *Appl. Surf. Sci.* 425 (2017) 750–757, <https://doi.org/10.1016/j.apsusc.2017.07.098>.
- [57] S. Bhaskar, E.W. Awini, K.C.H. Kumar, A. Lale, S. Bernard, R. Kumar, Design of nanoscaled heterojunctions in precursor-derived t-ZrO<sub>2</sub>/SiOC(N) nanocomposites: transgressing the boundaries of catalytic activity from UV to visible light, *Sci. Rep.* 10 (2020) 430, <https://doi.org/10.1038/s41598-019-57394-8>.
- [58] C. Stabler, A. Reitz, P. Stein, B. Albert, R. Riedel, E. Ionescu, Thermal properties of SiOC glasses and glass ceramics at elevated temperatures, *Materials* 11 (2018) 279, <https://doi.org/10.3390/ma11020279>.
- [59] Y. Blum, G.D. Soraru, A.P. Ramaswamy, D. Hui, S.M. Carturan, Controlled mesoporosity in SiOC via chemically bonded polymeric “spacers”, *J. Am. Ceram. Soc.* 96 (2013) 2785–2792, <https://doi.org/10.1111/jace.12485>.
- [60] K.M. Khalil, A.A. Elsamahy, M.S. Elanany, Formation and characterization of high surface area thermally stabilized titania/silica composite materials via hydrolysis of titanium (IV) tetra-isopropoxide in sols of spherical silica particles, *J. Colloid Interface Sci.* 249 (2002) 359–365, <https://doi.org/10.1006/jcis.2002.8268>.
- [61] B. Hahn, R. Weissmann, P. Greil, Electron paramagnetic resonance investigation of carbon distribution in SiOC glasses, *J. Mater. Sci. Lett.* 15 (1996) 1243–1244, <https://doi.org/10.1007/BF00274388>.
- [62] V. Ahilan, G.D. Bhowmick, M.M. Ghangrekar, M. Wilhelm, K. Rezwani, Tailoring hydrophilic and porous nature of polysiloxane derived ceramer and ceramic membranes for enhanced bioelectricity generation in microbial fuel cell, *Ionics* 25 (2019) 5907–5918, <https://doi.org/10.1007/s11581-019-03083-5>.
- [63] V. Petrovic, V. Ducman, S.D. Skapin, Determination of the photocatalytic efficiency of TiO<sub>2</sub> coatings on ceramic tiles by monitoring the photodegradation of organic dyes, *Ceram. Int.* 38 (2012) 1611–1616, <https://doi.org/10.1016/j.ceramint.2011.09.050>.
- [64] J. Zita, J. Krysa, U. Cernigoj, U. Lavrencic-Stangar, J. Jirkovsky, J. Rathousky, Photocatalytic properties of different TiO<sub>2</sub> thin films of various porosity and titania loading, *Catal. Today* 161 (2011) 29–34, <https://doi.org/10.1016/j.cattod.2010.11.084>.
- [65] I.N. Martyanov, K.J. Klabunde, Comparative study of TiO<sub>2</sub> particles in powder form and as a thin nanostructured film on quartz, *J. Catal.* 225 (2004) 408–416, <https://doi.org/10.1016/j.jcat.2004.04.019>.
- [66] K. Ranjith, R.R. Kumar, Regeneration of an efficient, solar active hierarchical ZnO flower photocatalyst for repeatable usage: controlled desorption of

poisoned species from active catalytic sites, RSC Adv. 7 (2017) 4983–4992,  
<https://doi.org/10.1039/C6RA27380G>.